Digital Breast Tomosynthesis Reconstruction with Detector Blur and Correlated Noise

Jiabei Zheng*, Jeffrey A. Fessler*, Heang-Ping Chan†

***Abstract*—This paper describes a new reconstruction method for digital breast tomosynthesis (DBT). The new method incorporates detector blur into the forward model. The detector blur introduces correlation in the measurement noise. We formulate it as a regularized quadratic optimization problem with data-fit term that accounts for the non-diagonal noise covariance matrix. By making a few assumptions based on the breast imaging process, we can model the detector blur in the optimization problem and solve it with a separable quadratic surrogate (SQS) algorithm. This method was applied to DBT reconstruction of breast phantoms and human subjects. The contrast-to-noise ratio and sharpness of microcalcifications and the visual quality of mass margins were analyzed and compared to those by the simultaneous algebraic reconstruction technique (SART). The results demonstrated the potential of the new method in improving the image quality of the reconstructed DBT images. This work is our preliminary step towards a model-based iterative reconstruction (MBIR) for DBT.**

***Index Terms*—Digital breast tomosynthesis, detector blur, correlated noise, model-based iterative reconstruction**

I. Introduction

Digital breast tomosynthesis (DBT) has been developed to reduce the problem of overlapping tissue in conventional 2-D mammography. In DBT, commonly-used reconstruction methods include filtered back-projection, the maximum-likelihood expectation-maximization algorithm [1][2] and simultaneous algebraic reconstruction technique (SART) [3]. These methods do not account for noise correlation or other image degradation factors in the imaging process. In this paper, we introduce a new reconstruction method that includes a correlated noise model, as a first step towards model-based iterative reconstruction (MBIR) for DBT.

In an x-ray imaging system, the finite pixel size and light diffusion in the phosphor of an indirect detector contribute to blurring of the measured image. Neglecting detector blur introduces blurring to the reconstructed objects, especially for small objects such as microcalcification (MC) in DBT. We modeled the detector blur and the associated noise correlation into the cost function of the optimization problem. The optimization problem is simplified with a few assumptions and solved with a slightly modified separable quadratic surrogate (SQS) method [4].

In this paper, we first introduce our detector blur model and the assumptions used for its simplification. We describe the optimization problem and the cost function for regularized reconstruction. The usefulness of the method is demonstrated by comparing its reconstructed image quality with that by SART using DBT of both breast phantom and human subject.

* Jiabei Zheng and Jeffrey A. Fessler are with the Department of Electrical and Computer Engineering, University of Michigan, Ann Arbor, MI. (e-mail: {jiabei,fessler}@umich.edu)

† Heang-Ping Chan is with the Department of Radiology, University of Michigan, Ann Arbor, MI. (e-mail: chanhp@med.umich.edu)

II. Methods

A. Formulation of the Reconstruction Problem

Let $\mathbf{A}_i$ denote the projector and $\mathbf{f}$ denote the unknown array of attenuation coefficients in the imaged volume. Let $\mathbf{Y}_i$ denote the measured projection at the ith projection angle of all m projections ($i = 1, ..., m$). Considering the detector blur, the expected projection value $\bar{\mathbf{Y}}_i$ can be written as

$$\bar{\mathbf{Y}}_i = I_0 \mathbf{B}_i \exp(-\mathbf{A}_i \mathbf{f}) \tag{1}$$

where $\mathbf{B}_i$ denotes the blurring operation in matrix form and I_0 is the constant expected projection value if there is no object present in the imaged volume. $\mathbf{B}_i$ is assumed to be projection-angle-dependent but linear shift-invariant within a given projection.

To deal with the non-diagonal matrix $\mathbf{B}_i$ before the exponential, we assume that the image f consists of two parts: (1) a low-frequency background $\mathbf{f}_\mathrm{b}$ that is approximately uniform within the support of the blurring kernel; (2) small structures $\mathbf{f}_\mathrm{s}$ (such as MC in DBT) that only contributes very little to the projection value ($\mathbf{A}_i \mathbf{f}_\mathrm{s} \ll 1$). These assumptions are more reasonable in breast imaging than in CT of body parts that include bone or other high-attenuation objects. Under these assumptions, we can approximate (1) as:

$$\bar{\mathbf{Y}}_i \approx I_0 \exp(-\mathbf{B}_i \mathbf{A}_i \mathbf{f}) \tag{2}$$

Thus the expectation of the transformed projection $\mathbf{y}_i$ is:

$$\bar{\mathbf{y}_i} = \log\left(I_0 / \mathbf{Y}_i\right) \approx \mathbf{B}_i \mathbf{A}_i \mathbf{f} \tag{3}$$

We assume $\mathbf{y}_i$ has approximately a multivariate Gaussian distribution: $\mathbf{y}_i \sim \mathcal{N}(\bar{\mathbf{y}}_i, \mathbf{K}_i)$. $\mathbf{K}_i$ is the covariance matrix for the ith projection.

The quantum noise in the imaging process is affected by the detector blur but the detector electronic noise is not. A reasonable model for the noise covariance $\mathbf{K}_i$ is:

$$\mathbf{K}_i = \mathbf{B}_i \mathbf{K}_i^q \mathbf{B}_i' + \mathbf{K}_i^r \tag{4}$$

where $'$ denotes conjugate transpose (in case the kernel of $\mathbf{B}_i$ is asymmetric). $\mathbf{K}_i^q$ and $\mathbf{K}_i^r$ are diagonal matrices of the variances of quantum noise and readout noise at each detector element, respectively.

We then formulate the following reconstruction problem:

$$\begin{aligned} \hat{\mathbf{f}} &= \arg\min_{\mathbf{f}} \frac{1}{2} \sum_i \|\mathbf{y}_i - \mathbf{B}_i \mathbf{A}_i \mathbf{f}\|^2_{(\mathbf{B}\mathbf{K}_i^q \mathbf{B}' + \mathbf{K}_i^r)^{-1}} + R(\mathbf{f}) \\ &= \arg\min_{\mathbf{f}} \frac{1}{2} \sum_i \|\mathbf{P}_i \mathbf{y}_i - \mathbf{P}_i \mathbf{B}_i \mathbf{A}_i \mathbf{f}\|_2^2 + R(\mathbf{f}) \end{aligned} \tag{5}$$

where $R(\mathbf{f})$ is the regularization term and the inverse matrix square root of the noise covariance is

$$\mathbf{P}_i = (\mathbf{B}_i \mathbf{K}_i^q \mathbf{B}_i' + \mathbf{K}_i^r)^{-1/2} \tag{6}$$

B. Implementation of $\mathbf{P}_i$

Since $(\mathbf{B}_i\mathbf{K}_i^q\mathbf{B}_i' + \mathbf{K}_i^r)$ is non-diagonal, the implementation of $\mathbf{P}_i$ is very challenging. In CT application, one possible method is to solve another optimization problem with a set of conjugate gradient iterations [5]. In DBT, we can dramatically simplify the implementation by making some reasonable assumptions. Unlike body CT where there exist large bones and even perhaps metal objects of significant size that are strongly attenuating, the compressed breast has a fairly uniform thickness mainly composed of soft tissue. As a first-order approximation, we assume quantum noise to be constant for all detector elements in a given projection angle:

$$\mathbf{K}_i^q = \sigma_i^{q2}\mathbf{I} \tag{7}$$

In addition, we assume all detector elements have similar readout noise variance:

$$\mathbf{K}_i^r = \sigma_i^{r2}\mathbf{I} \tag{8}$$

Let $\mathbf{h}_i$ be the point spread function (PSF) of the detector, The blurring operation is given by $\mathbf{B}_i = \mathbf{Q}^{-1}\mathbf{H}_i\mathbf{Q}$, where $\mathbf{Q}$ is the discrete Fourier Transform (DFT) matrix and $\mathbf{H}_i = \mathrm{Diag}(\mathrm{DFT}\{\mathbf{h}_i\})$. Then the operation $\mathbf{P}_i$ by a vector can be easily implemented as a high-pass filter using FFT operations without needing any iterative method for matrix inversion:

$$\mathbf{P}_i = \mathbf{Q}^{-1}(\sigma_i^{q2}\mathbf{H}_i\mathbf{H}_i' + \sigma_i^{r2}\mathbf{I})^{-1/2}\mathbf{Q} \tag{9}$$

In our study, we used a Lucite slab with a similar thickness as the object to be reconstructed to estimate σ_i^q. σ_i^r was estimated from the dark current image of the detector.

C. Regularization

Since $\mathbf{P}_i$ is implemented as a high-pass filter, it would amplify noise in reconstruction if used without regularization. Regularization is very important for stable reconstruction. We use a Huber-like function $\eta(t)$ to define $R(\mathbf{f})$ in this work:

$$\eta(t) = \delta^2(\sqrt{1 + (t/\delta)^2} - 1) \tag{10}$$

Since the DBT reconstruction is non-isotropic, the regularization term is written separately in terms of the horizontal and vertical in-plane directions as

$$R(\mathbf{f}) = \beta_x \sum_j \eta([\mathbf{C}_x\mathbf{f}]_j) + \beta_y \sum_j \eta([\mathbf{C}_y\mathbf{f}]_j) \tag{11}$$

where $\mathbf{C}_x$ and $\mathbf{C}_y$ are operations to calculate difference between neighboring pixels along the x and y-direction, respectively, as defined in Fig. 1. Our DBT slice thickness is 10 times in-plane pixel size, making correlation between slices relatively weak and z-direction regularization unnecessary.

D. The Reconstruction Algorithm

Both the quadratic function of the data-fit term and $\eta(t)$ are convex and their second-order derivatives are less than or equal to 1. This allows us to use SQS with a small modification to account for the effective system matrix $\tilde{\mathbf{A}}$ and solve the optimization problem:

$$\begin{aligned}\mathbf{f}^{(n+1)} = \mathbf{f}^{(n)} - \big(&\beta_x\mathbf{C}_x'\dot{\eta}(\mathbf{C}_x\mathbf{f}^{(n)}) + \beta_y\mathbf{C}_y'\dot{\eta}(\mathbf{C}_y\mathbf{f}^{(n)}) \\ &+ \tilde{\mathbf{A}}'(\tilde{\mathbf{A}}\mathbf{f}^{(n)} - \tilde{\mathbf{y}})\big) \oslash \big(4\beta_x\mathbf{1} + 4\beta_y\mathbf{1} + |\tilde{\mathbf{A}}'\tilde{\mathbf{A}}|\mathbf{1}\big)\end{aligned} \tag{12}$$

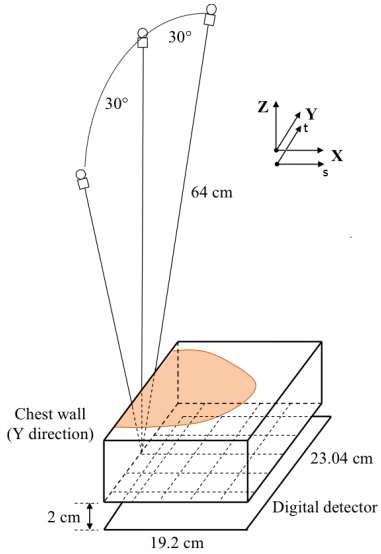

Fig. 1: Geometry of the DBT system used in this study.

where $\mathbf{1}$ is an all-one vector, $|\cdot|$ and $\oslash$ represent element-wise absolute value and division, and the effective system matrix is defined as

$$\tilde{\mathbf{A}} = \begin{pmatrix} \tilde{\mathbf{A}}_1 \\ \dots \\ \tilde{\mathbf{A}}_m \end{pmatrix} = \begin{pmatrix} \mathbf{P}_1\mathbf{B}_1\mathbf{A}_1 \\ \dots \\ \mathbf{P}_m\mathbf{B}_m\mathbf{A}_m \end{pmatrix} \tag{13}$$

$$\tilde{\mathbf{y}} = \begin{pmatrix} \tilde{\mathbf{y}}_1 \\ \dots \\ \tilde{\mathbf{y}}_m \end{pmatrix} = \begin{pmatrix} \mathbf{P}_1\mathbf{y}_1 \\ \dots \\ \mathbf{P}_m\mathbf{y}_m \end{pmatrix} \tag{14}$$

$\mathbf{P}_i$ is a high-pass filter with negative elements in its PSF. $\tilde{\mathbf{A}}$ has negative elements, making it challenging to implement $|\tilde{\mathbf{A}}'\tilde{\mathbf{A}}|\mathbf{1}$. The implementation of $|\tilde{\mathbf{A}}'\tilde{\mathbf{A}}|\mathbf{1}$ is still under investigation. We temporarily use $\tilde{\mathbf{A}}'\tilde{\mathbf{A}}\mathbf{1}$ as an approximation.

In DBT reconstruction, we usually use only one projection view at a time. Therefore, we assume that, for each i:

$$\nabla(\sum_{k=1}^{m} \|\tilde{\mathbf{y}}_k - \tilde{\mathbf{A}}_k\mathbf{f}\|_2^2) \approx m\nabla(\|\tilde{\mathbf{y}}_i - \tilde{\mathbf{A}}_i\mathbf{f}\|_2^2) \tag{15}$$

The ordered-subset (OS) reconstruction update is given by:

$$\mathbf{f}^{(n,i+1)} = \mathbf{f}^{(n,i)} - \nabla\Psi_i(\mathbf{f}^{(n,i)}) \oslash \big(4\beta_x\mathbf{1} + 4\beta_y\mathbf{1} + |\tilde{\mathbf{A}}'\tilde{\mathbf{A}}|\mathbf{1}\big) \tag{16}$$

$$\nabla\Psi_i(\mathbf{f}^{(n,i)}) = \beta_x\mathbf{C}_x'\dot{\eta}(\mathbf{C}_x\mathbf{f}^{(n,i)}) + \beta_y\mathbf{C}_y'\dot{\eta}(\mathbf{C}_y\mathbf{f}^{(n,i)}) + m\tilde{\mathbf{A}}_i'(\tilde{\mathbf{A}}_i\mathbf{f}^{(n,i)} - \tilde{\mathbf{y}}_i) \tag{17}$$

The iteration counter n is incremented by 1 after all measured projections have been used once.

III. Materials

A. DBT System

We used a GE GEN2 prototype DBT system for image acquisition. The imaging geometry is shown in Fig. 1. The system uses a CsI phosphor/a:Si active matrix flat panel detector with a pixel size of 0.1mm×0.1mm and an area of 1920×2304 pixels. The detector is enclosed inside the breast support and is stationary during image acquisition. The distance from the x-ray source to the fulcrum is 64cm. There is a 2cm gap between the imaged volume and the digital detector.

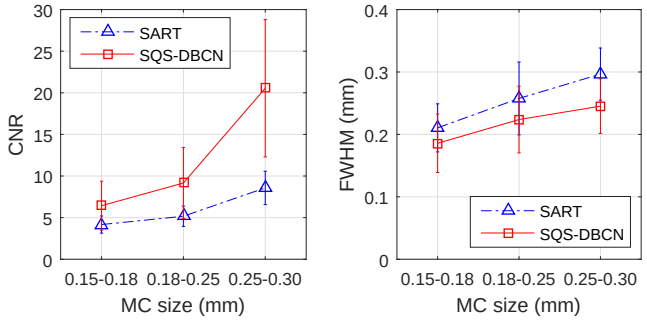

Fig. 3: Comparison of the mean CNR and mean FWHM averaged over all clusters in the phantom.

B. Breast Phantom and Human Subject DBT

MCs are small calcium deposits in the breast of sizes from about 0.1mm to 0.5mm. Clustered MCs are important signs of early breast cancer. One of the main challenges in DBT reconstruction is to reduce noise while enhancing MCs and preserving the margin features of masses. In this study, we used a breast phantom with embedded MCs for the evaluation of the effects of reconstruction methods and parameters on the image quality of MCs. It is difficult to build mass phantoms with realistic spiculated or ill-defined margins, which are strong indicators of breast cancer; we therefore used real breast DBT for visual evaluation of the image quality of masses.

The breast phantom consists of a stack of five 1-cm-thick slabs of breast tissue mimicking material [6]. Clusters of calcium carbonate specks of three nominal size ranges (0.15-0.18mm, 0.18-0.25mm, and 0.25-0.30mm) were sandwiched between the slabs to simulate MCs of different conspicuity levels. For the human subject DBT, we selected a case with a spiculated mass that was biopsy-proven to be an invasive ductal carcinoma. Both the phantom and human subject DBT were acquired with 60° scan angle, 3° increments and 21 projections. To simulate the DBT acquired with a GE commercial system, we used the 9 central projections for reconstruction, corresponding to DBT of 24° scan angle with 3° increments.

C. Figures of Merit (FOMs)

Quantitative comparison of reconstruction quality are based on two FOMs of MCs: contrast-to-noise ratio (CNR) and full-width at half maximum (FWHM). We applied a 2-D least-squares Gaussian fitting to each reconstructed MC. With the fitted standard deviation σ_{MC}, the FWHM is given by $2.355\sigma_{\mathrm{MC}}$. The noise level σ_{NP} is estimated from a noise patch near each cluster. The CNR is given as: $\mathrm{CNR} = A_{\mathrm{MC}}/\sigma_{\mathrm{NP}}$, where A_{MC} is the fitted amplitude of the MC.

IV. Results and Discussion

A. Reconstructed MC Clusters

We compared the new method (SQS with detector blur and correlated noise, or SQS-DBCN) with SART. We performed three complete iterations for SART since more iterations will amplify noise and reduce the CNR of MCs. Compared with SART, SQS-DBCN is regularized, allowing us to increase the number of iterations and enhance the contrast of MCs. We

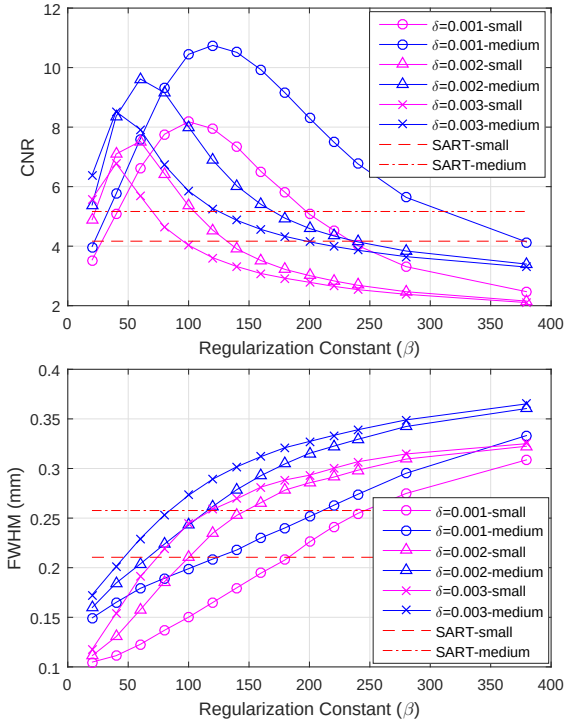

Fig. 4: Parameter selection: CNR and FWHM as a function of β for a range of δ. The red lines indicate the level of the SART.

experimentally chose 10 complete iterations for this study. To reduce the number of the parameters to be determined, we also set $\beta_x = \beta_y = \beta$. For the discussion in this section, the parameter combination is: $\beta = 80$, $\delta = 0.002/\mathrm{mm}$.

The reconstructed clusters are shown in Fig. 2. To make a more quantitative comparison, we used 49 of 0.15-0.18mm MCs, 66 of 0.18-0.25mm MCs and 64 of 0.25-0.30mm MCs from 5 clusters of each size. We calculated the mean CNR and FWHM of the MCs in each size range. The results are shown in Fig. 3. Compared with SART, SQS-DBCN generates more conspicuous and sharper MCs, as indicated by a higher CNR and smaller FWHM. For the smallest MCs (0.18-0.25mm), the mean CNR increases by 54.4% from 4.17 to 6.44 using the SQS-DBCN reconstruction. The mean CNRs increased by 77.3% and 139.7% for medium and large MCs. With SART, the FWHMs of the reconstructed MCs are larger than their nominal size. With the SQS-DBCN method, the FWHMs are closer to the nominal size, due to the 'shrink' effect of the deblurring by $\mathbf{P}_i$. The regularization suppressed background noise, making MCs more visible to the observer.

B. Regularization Parameter Selection

Performance of the method depends on parameter selection of the regularization term. We reconstructed the phantom DBT with different parameter combinations. Mean CNR and FWHM were calculated for each reconstruction and the trends are shown in Fig. 4. For MCs of different sizes, there exists a different 'optimal' parameter combination that yields maximum CNR. Over a large range of parameters, the new method outperforms the SART method in the sense of enhancing CNR.

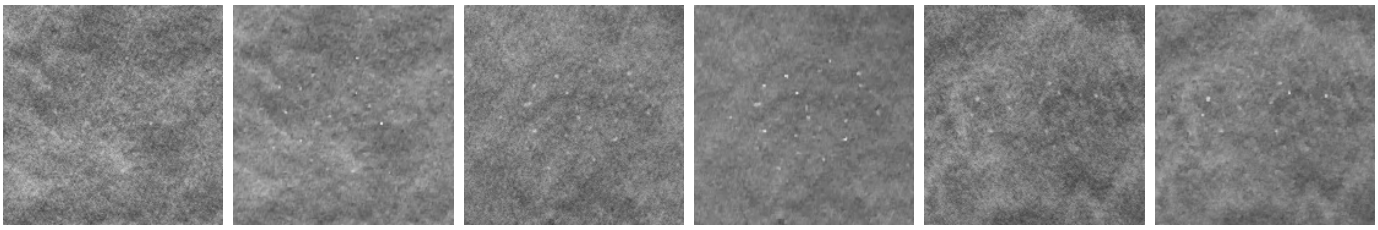

(A1) Cluster A: SART: mean CNR = 3.87, FWHM = 0.210mm | (A2) Cluster A: SQS: mean CNR = 6.86, FWHM = 0.172mm | (B1) Cluster B: SART: mean CNR = 5.56, FWHM = 0.235mm | (B2) Cluster B: SQS: mean CNR = 10.4, FWHM = 0.217mm | (C1) Cluster C: SART: mean CNR = 5.55, FWHM = 0.243mm | (C2) Cluster C: SQS: mean CNR = 8.37, FWHM = 0.222mm

Fig. 2: (A1)-(C2) shows the comparison of MC clusters. Mean CNR and FWHM of all MCs on the patch are given under each figure. (A1)(B1)(C1) used SART with 3 iterations, (A2)(B2)(C2) used SQS-DBCN with $\beta = 80$, $\delta = 0.002/mm$, 10 iterations. Size of MCs in Cluster A is 0.15-0.18mm, size of MCs in Cluster B and C is 0.18-0.25mm.

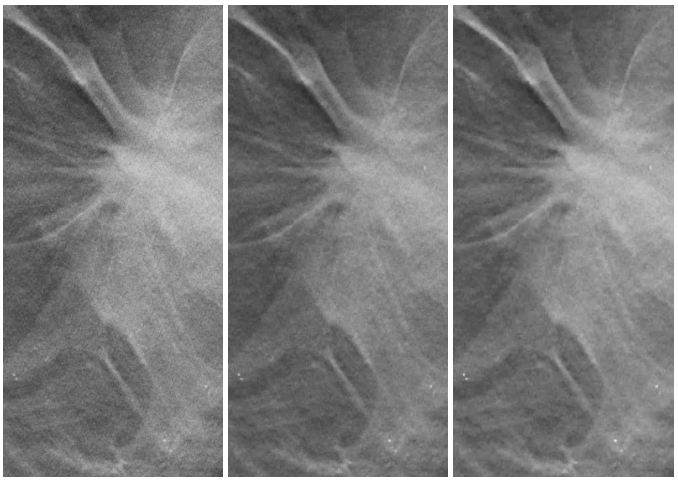

(a) SART, 3 iterations | **(b)** SQS-DBCN, 10 iterations, $\beta = 80$, $\delta = 0.002/\mathrm{mm}$ | **(c)** SQS-DBCN, 10 iterations, $\beta = 120$, $\delta = 0.001/\mathrm{mm}$

Fig. 5: Comparison of reconstructed images for human subject DBT. The CNR of MCs increases from image (a) to (c). However, the spiculation and the tissue textures become more patchy and artificial in (c). The artifacts may not be readily visible in this reduced-size image.

The FWHM of all MCs increases as β increases due to the stronger smoothing effect from the regularization term.

The parameter combination used for reconstructing the examples in Fig. 2 was not the one with highest CNR shown in Fig. 4 to avoid the strong distortion of the background texture in the images (also see Fig. 5(c)).

C. Human Subject DBT

The FOMs used in this study only evaluated the CNR and FWHM of MCs. Currently there is no simple FOM that can describe the visual quality of the mass margin and tissue texture. Some reconstruction methods or parameter combinations can generate strong artifacts on the tissue texture, as observed in CT [7]. To evaluate the visual quality of the tissue texture, we applied SQS-DBCN to the human subject DBT. Fig. 5 shows a comparison of two parameter combinations to SART. It can be observed that the SQS-DBCN method enhanced MCs by the parameter combination ($\beta = 80$, $\delta = 0.002/mm$) (Fig. 5(b)), preserved tissue structure and did not generate noticeable artifact compared to the image by ($\beta = 120$, $\delta = 0.001/mm$) (Fig. 5(c)), in which the texture looks patchy and artificial. Therefore, the former is a better choice for human DBT although the latter provided higher CNR enhancement for MCs. We are investigating parameter selection strategies that can be more adaptive to different imaging conditions and for various breast lesions and parenchymal densities.

V. Conclusion

We proposed a DBT reconstruction method that incorporates detector blur and a correlated noise model as the first step towards developing a model-based iterative reconstruction method for DBT. We have shown quantitatively and visually that the new SQS-DBCN method can better enhance MCs compared with the SART while preserving the image quality of spiculations and tissue texture.

The SQS-DBCN method depends on several assumptions. The performance of the method depends on good parameter selection and accurate estimation of noise variance. Further study is underway to develop an adaptive method to select the parameters, better estimation of noise variance, and more general model to relax the assumptions.

Acknowledgment

This work is supported by National Institutes of Health grant number R01 CA151443.

References

[1] K. Lange and J. A. Fessler, *Globally Convergent Algorithms for Maximum a Posteriori Transmission Tomography*, IEEE Trans Image Processing, vol. 4, pp. 1430-1438, 1995.

[2] T. Wu, et al., *Tomographic Mammography Using a Limited Number of Low-dose Cone-beam Projection Images*, Medical Physics, vol. 30, pp. 365-380, 2003.

[3] Y. Zhang, H.-P. Chan, B. Sahiner, et al, *A Comparative Study of Limited-angle Cone-beam Reconstruction Methods for Breast Tomosynthesis*, Medical Physics, vol. 33, pp. 3781-3795, 2006.

[4] H. Erdogan and J. A. Fessler, *Ordered Subsets Algorithms for Transmission Tomography*, Physics in Medicine and Biology, vol. 44, pp. 2835-2851, 1999.

[5] J. W. Stayman, et al., *Generalized Least-Squares CT Reconstruction with Detector Blur and Correlated Noise Models*, Proc. SPIE, vol. 9033, 903335, 2014.

[6] H.-P. Chan, M. Goodsitt, et al., *Digital Breast Tomosynthesis: Observer Performance of Clustered Microcalcification Detection on Breast Phantom Images Acquired with an Experimental System Using Variable Scan Angles, Angular Increments, and Number of Projection Views*, Radiology 273, 675-685, 2014.

[7] F. E. Boas and D. Fleischmann, *CT Artifacts: Causes and Reduction Techniques*, Imaging in Medicine, vol. 4, pp. 229-240, 2012.